A Two-Layer Central Pattern Generator for Human Locomotion Control

by

Ties Schukking

Student Number:	5648645
Faculty:	Mechanical Engineering, TU Delft
Track:	BioMechanical Design
Daily Supervisor:	Dr. Matthew Mulligan
General Supervisor:	Dr. Ir. Eline van der Kruk
External Committee Member:	Dr. Ir. Winfred Mugge
Year:	2026

TU Delft

A Two-Layer Central Pattern Generator for Human Locomotion Control

Ties Schukking
Delft University of Technology
Delft, Netherlands

1. Abstract

Background and Objective: Human walking is governed by the interaction between central pattern generators (CPGs), reflexes and the vestibular system. While single-layer CPG models like the Unit Burst Generator (UBG) are commonly used in simulations, they couple oscillation frequency and amplitude, limiting control of gait velocity. This study evaluates a two-Layer UBG (TLU) architecture, which decouples these properties, to determine its efficacy in producing realistic human gait and its ability to control gait velocity. **Method:** A 2D musculoskeletal model (9 DOF, 18 muscles) was controlled by the UBG or TLU architecture during gait, integrated with muscle reflexes and vestibular feedback. Additionally, velocity control was assessed by optimizing specific CPG parameters to increase walking speed. **Results:** Both controllers produced stable, physiologically plausible gait that aligned well with normative data. Neural analysis showed that while reflexes mainly controlled lower leg muscles, the CPG was essential for the loading response in muscles spanning the knee and hip joints. In the velocity control, the TLU model could reach higher gait velocities with fewer optimization parameters compared to the UBG. **Conclusion** The CPG effectively coordinates with muscle reflexes and vestibular feedback to produce human-like gait, complementing where the other neural control mechanisms fall short. The TLU provides a more efficient mechanism for gait modulation than the UBG by separating frequency and amplitude control.

2. Introduction

Human walking appears effortless, yet it requires precise coordination between muscles and neural control structures. Neurophysiological studies suggest that human locomotion is in part controlled by a neural structure known as the central pattern generator (CPG). Since Graham Brown first introduced the concept in 1911 [1], CPGs have been identified across a wide range of species [2]–[4], including humans [3], [5], [6], where their existence and contribution to locomotor rhythm generation are generally acknowledged. However, their precise role, and how they interact with other neural control mechanisms such as reflex pathways and the vestibular system, remains unclear.

Because the exact role of CPGs in human locomotion, their neural architecture and the specific mechanisms by which they integrate peripheral feedback signals remain unclear, numerous attempts have been made to gain insight into the CPG's working mechanisms through predictive simulations. The CPG model most frequently used is the Unit Burst Generator (UBG) [2]. This is a network of half-center oscillators where each oscillator controls the muscles around a specific joint (Fig. 1). By connecting multiple oscillators, stable phase relationships emerge, synchronizing their activity. This neural architecture has been shown to be effective in controlling bipedal musculoskeletal models [7]–[12].

However, a new model has been introduced by Rybak et al. [13], which consists of two control layers. In the UBG architecture, each joint is governed by a half-centre oscillator that determines both the frequency and the amplitude (or shape) of the oscillations. In contrast, the new model decouples these properties by introducing two distinct layers: a rhythm generation layer and a pattern formation layer (Fig. 2).

This model is similar to the UBG model, however, the rhythm generation layer is now added. The model will hereafter be referred to as the two-layer UBG (TLU) model. The separation through these layers provides independent control of frequency and muscle excitation levels (i.e. amplitude and shape), which allows for easier modulation of walking velocity with fewer control parameters compared to the UBG architecture. This is consistent with the general view that human locomotion relies on modular control strategies, in which a small number of control parameters modulate a general locomotion pattern to produce different walking speeds [14]–[16].

Whether this combined CPG architecture reflects the actual neural structure in the human body and whether it can control bipedal locomotion remains unclear. The two studies that implemented the TLU either used a skeletal

model with torque actuators instead of muscles [17] or a highly simplified musculoskeletal biped consisting of a single segment per leg and two muscles at the hip joint [18]. Moreover, the extent to which the CPG serves as the primary neural controller of human gait remains debated, as purely reflex-based models have also been successful in generating bipedal locomotion in forward simulations [19].

Whether the TLU model can reproduce realistic human gait patterns and whether its two-layered structure enables control of gait velocity using a small set of parameters, would provide support for a two-layer organization in human CPGs. Therefore, the primary aim for this thesis is to evaluate the performance of the TLU controller in predictive simulations. This will be addressed through the following three objectives: (1) to determine whether the novel TLU controller produces more realistic human gait than the established one-layer UBG controller; (2) to investigate the relative roles of the CPG, reflexes and vestibular feedback in motor control of human gait; and (3) to assess whether the separation of frequency and amplitude in the two-layer architecture of the TLU controller, enables control of gait velocity using less parameters compared to the UBG model.

3. Method

In this section, all model components are described in Sections 3.1 to 3.5, beginning with the musculoskeletal model, followed by the neuronal architectures, neuron model, feedback signals and the gait phases. Next, the general optimization method is presented in Section 3.6, followed by the optimization procedures used to address the first two objectives (Section 3.7) and the final objective (Section 3.8). Finally, Section 3.9 describes the validation method.

3.1. Musculoskeletal model

A two-dimensional sagittal-plane musculoskeletal model (H0918v3.hfd) [20] was used in the predictive simulations, representing a 1.70 m, 74.5 kg male. The model is comprised of seven rigid bodies (feet, shanks, thighs, and a combined pelvis–torso segment) with nine degrees of freedom: pelvic tilt, pelvic translation in the horizontal and vertical directions, and flexion/extension at the hip, knee and ankle joints. Eighteen Hill-type muscle–tendon units actuate the model, including the Iliopsoas (IP), Gluteus Maximus (GMAX), Rectus Femoris (RF), Hamstrings (HAM), Vastus (VAS), Biceps Femoris short head (BFSH), Gastrocnemius (GAS), Soleus (SOL), and Tibialis Anterior (TA) for both legs. Ground contact is modelled via 0.06 m-diameter contact spheres placed at the heels and toes, interacting with the ground through a nonlinear spring–damper system (static friction = 0.9, dynamic friction = 0.6, stiffness = 11006.4N/m, damping = Ns/m).

3.2. CPG structure

Two CPG controllers were developed: the UBG and TLU whose neuronal structure will be described in Section 3.2.1 and Section 3.2.2 respectively.

3.2.1. UBG

The UBG architecture was inspired by Taga et al. (1991) [21]. In the UBG controller (Fig. 1), muscles spanning each joint are controlled by a half-center oscillator composed of a flexor and an extensor neuron, projecting to the corresponding flexor and extensor muscles. Within a leg, synchronization between half-centers is achieved via inhibitory connections from the hip flexor (H-F) and extensor (H-E) neurons to the knee and ankle extensor neurons (K-E, A-E). Interlimb coordination is achieved through mutual inhibitory connections between the hip flexor and extensor neurons of both legs

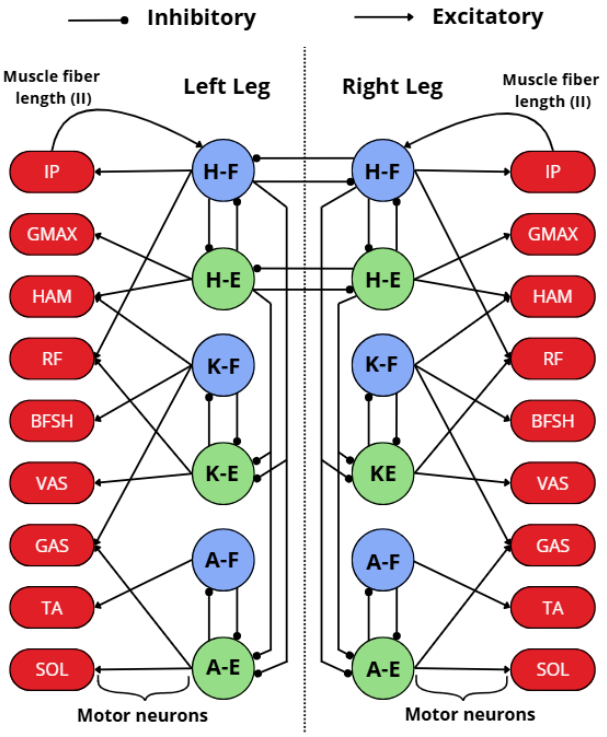

Fig. 1. Neuronal architecture of the UBG controller. Green neurons represent the extensor group and blue neurons the flexor group. H = hip, K = knee, A = ankle, E = extensor, F = flexor.

3.2.2. TLU

In the TLU controller (Fig. 2), rhythmic activity is generated by a single, more extensive half-center oscillator forming the rhythm generation layer. Mutual inhibition between the rhythm generation flexor (RG-

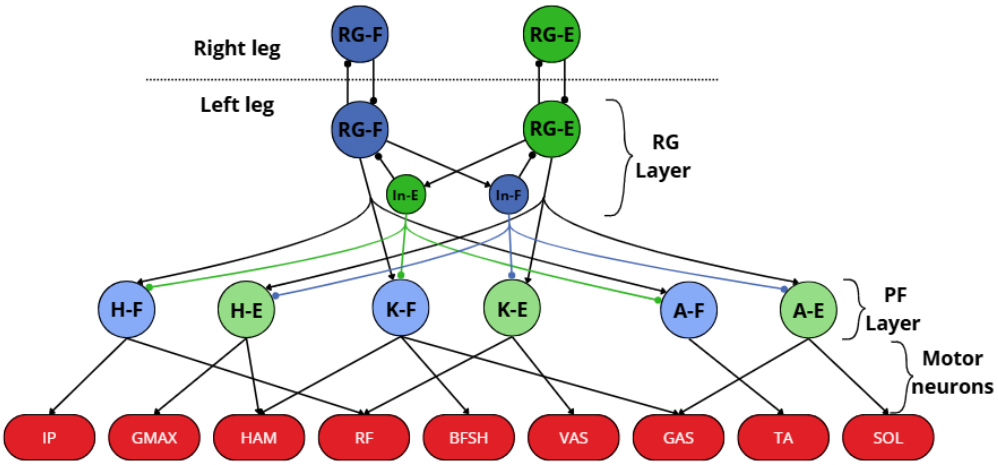

Fig. 2. Neuronal architecture of the TLU controller. The full structure of the left leg is shown; for the right leg, only the rhythm generation layer neurons and their connections to the left leg are depicted. Green neurons represent the extensor group and blue neurons the flexor group. Colored connections are used for visual clarity only and are functionally equivalent to black connections. RG = rhythm generation, PF = pattern formation, In = inter neuron, E = extensor, F = flexor.

F) and extensor (RG-E) neurons is mediated by interneurons (In-F, In-E). Neurons in the pattern formation layer receive excitatory input from the RG neuron of the same group and inhibitory input from the interneuron of the opposing group. Interlimb coordination is achieved through mutual inhibitory connections between the RG-F and RG-E neurons of both legs.

3.3. Neuron model

Neuronal dynamics were modeled using the Matsuoka oscillator [22], [23]. Each neuron is described by two coupled first-order differential equations (Eq. 1, Eq. 2) representing the membrane potential and neural adaptation, with the output defined in Eq. 3. The model has two state variables: u_i, representing the membrane potential and f_i, representing adaptation of the i-th neuron. The variables y_i iand y_j denote the outputs of the i-th and j-th neurons, respectively. The time constants τ_{r_i} and τ_{a_i} determine the response speed and adaptation lag. The tonic input is given by s_0 and the parameters b and w_{ij} define the strengths of sensory feedback and interneuronal coupling respectively.

$$\tau_{r_i} \frac{du_i}{dt} = -u_i + \sum_{j=1}^{n} w_{ij} y_j + s_0 - b f_i + \text{feed}_i \tag{1}$$

$$\tau_{a_i} \frac{df_i}{dt} = -f_i + y_i \tag{2}$$

$$y_i(u_i) = \max(0, u_i) \tag{3}$$

3.4. Feedback signals

Two types of muscle feedback signals, representing muscle reflexes, were used to control the musculoskeletal model: muscle fiber length (type II) and muscle force (type Ib). These reflexes are defined in Eqs. 4 to 7.

$$II = w_{II} \cdot \max(0, l_{\text{norm}} - l_{\text{off}}) \tag{4}$$

$$Ib = w_{Ib} \cdot F_{\text{norm}} \tag{5}$$

With

$$l_{\text{norm}} = \frac{l}{l_{\text{opt}}} \tag{6}$$

$$F_{\text{norm}} = \frac{F}{F_{\text{max}}} \tag{7}$$

The variables w_{II} and w_{Ib} are the weights corresponding to each feedback signal. l_{norm} and F_{norm} represent the normalized fiber length and muscle force respectively with an offset (l_{off}) for the type II feedback. The normalized values are calculated by dividing the fiber length (l) and muscle force (F) by the optimal fiber length (l_{opt}) and maximum contractile muscle force (F_{max}) (Eq. 6 and Eq. 7).

Type Ib and II feedback is primarily implemented via excitatory monosynaptic reflexes to the ipsilateral muscle. An exception is made for the length feedback of the iliopsoas (IP) muscle. In addition to the monosynaptic pathway, the type II signal is projected to the hip flexor (H-F) neuron in the UBG controller and to the RG-F neuron in the TLU controller of the ipsilateral leg during the stance phase. This additional pathway is used to synchronize the CPG with the musculoskeletal system.

TABLE I

	Stance			Swing			Neural delay (ms)	
	VES	II	Ib	VES	II	Ib	VES	Ib & II
GMAX	x				x		50	10
IP	x	x*			x		50	10
HAM	x		x				50	15
RF	x						50	10
VAS			x		x			20
GAS		x	x		x			35
TA		x			x			35
SOL		x	x		x			35

Overview of reflex signals and associated neural delays for each muscle. VES includes both the torso angle (θ_{torso}) and its angular velocity (ω_{torso}). * indicates signals that are additionally fed directly into the CPG.

In addition to muscle reflexes, vestibular feedback was implemented. Muscles spanning the hip joint receive input derived from the torso angle and its angular velocity. The transformation of torso angle and angular velocity into vestibular feedback signals is defined in Eqs. 8 to 11.

$$VES^{\text{flex}}_{\text{ang}} = w^{\text{flex}}_{\text{ang}} \cdot \max(\theta_{\text{torso}} - \theta_{\text{ref}}, 0) \quad (8)$$

$$VES^{\text{ext}}_{\text{ang}} = w^{\text{ext}}_{\text{ang}} \cdot |\min(\theta_{\text{torso}} - \theta_{\text{ref}}, 0)| \quad (9)$$

$$VES^{\text{flex}}_{\text{vel}} = w^{\text{flex}}_{\text{vel}} \cdot \max(\omega_{\text{torso}}, 0) \quad (10)$$

$$VES^{\text{ext}}_{\text{vel}} = w^{\text{ext}}_{\text{vel}} \cdot |\min(\omega_{\text{torso}}, 0)| \quad (11)$$

The parameter w is the vestibular feedback gain, with subscripts and superscripts indicating the signal type (angle or angular velocity) and muscle group (flexor or extensor), respectively. The variables θ_{torso} and θ_{ref} are the torso angle and its reference value relative to the vertical, while ω_{torso} is the torso angular velocity.

Neural transmission delays were applied to both muscle and vestibular feedback pathways. Delay values were taken from [24] and are summarized in Table I, which also specifies which muscle reflexes are active during the stance and swing phases.

3.5. Gait Phases

Each gait cycle was divided into a stance and swing phase. The stance phase is initiated when the vertical ground reaction force exceeded 20% of total model weight. Phase-dependent control was implemented by assigning distinct weights to motor neurons, vestibular feedback and muscle reflex pathways. Parameters describing intrinsic neuron dynamics, CPG coupling weights, length offsets and the reference torso angle were held constant across phases.

3.6. General optimization method

The simulations and optimizations were performed using the SCONE software platform using the Covariance Matrix Adaptation Evolutionary Strategy [20] with a population size per generation of 10. The CPG network was modelled in a ScriptController and numerically integrated using a fourth-order Runge–Kutta scheme with a fixed time step of 0.005s.

3.7. Two-step optimization

In order to answer the first two objectives, a two-step optimization procedure was developed. During this optimization a cost function was minimized (Section 3.7.1). The two-step optimization procedure is described in Section 3.7.2), the determination of the initial conditions in Section 3.7.3) and the selection of the best solution in (Section 3.7.4).

3.7.1. Cost function

The optimization objective was to minimize a weighted sum of performance measures to achieve a stable gait pattern:

• Cost of transport: metabolic energy expenditure per unit distance [25] (see Appendix A for the full definition). Measure does not go to zero, but is minimized.

• Muscle activation: cubed muscle activation per unit distance. Measure does not go to zero, but is minimized.

• Ground reaction force: penalty for vertical ground reaction forces exceeding 1.4 times body weight. Measure is zero when the normalized ground reaction force curve is below 1.4.

• Gait term: penalizes walking velocities below a certain minimum velocity (1m/s) and gives a penalty if the model falls. Whenever the minimum velocity is reached and the model does not fall, the measure becomes zero.

• Joint angles: penalizes excessive ankle angles when exceeding physical limits. Measure is zero when all angles remain within range.

• Limit torque: penalizes limit torques of the knee. Measure is zero when no limit torques are generated.

• Periodicity: evaluates whether the CPG produces periodic signals in the absence of feedback signals. Periodicity is considered achieved when the peaks in the neuron states differ by less than 4% in amplitude

and the time between peaks differs by less than 4%. A penalty is applied when neurons do not exhibit periodic behavior, increasing with the number of neurons that fail to be periodic. If the frequency is below 0.83 Hz, an additional penalty is applied proportional to the difference between the current frequency and this minimum required frequency. The measure equals zero when the minimum frequency is reached and all neurons exhibit periodic behavior.

3.7.2. Procedure

A total of 83 parameters for the UBG controller and 105 parameters for the TLU controller were optimized. The type II feedback weight from the IP to the CPG was fixed at 1. The length offsets of the GMAX, IP, GAS, and SOL muscles were set to 0.9, 0.9, 1 and 1, respectively. An overview of the optimizable parameters is provided in Table II.

TABLE II

	UBG		**TLU**	
	Stance	*Swing*	*Stance*	*Swing*
Neuron dynamics ($\tau_{r_i}, \tau_{a_i}, s_0, b$)	24		40	
CPG coupling (w_{ij})	12		18	
Muscle feedback (w_{Ib}, w_{II})	8	5	8	5
Vestibular feedback ($w^{\text{flex}}_{\text{ang}}$, $w^{\text{ext}}_{\text{ang}}$, $w^{\text{ext}}_{\text{vel}}$, $w^{\text{ext}}_{\text{vel}}$)	8	0	8	0
Motor neuron weights	12	12	12	12
Length offset (l_{off})	1		1	
Reference torso angle (θ_{ref})	1		1	

Overview of optimizable parameters for the UBG and the TLU model.

Given the large dimensionality of the parameter space, a good initial guess is important for finding the optimal solution. To obtain the optimal solution, a two-step optimization procedure was used.

In the first step, a mimic objective was introduced that minimized the root mean square error between muscle excitation signals generated by a reflex-based controller during gait [19] and the weighted sum of excitation signals produced by the CPG, muscle reflexes and vestibular system (Fig. 3). To accelerate convergence, deviations of the CPG's frequency from the step frequency of the gait generated by the reflex controller (0.89 Hz), were penalized. In addition, the RMSE of the HAM and VAS excitations during initial contact was increased by a factor of 100 to emphasize accurate reproduction of the loading response of these muscles.

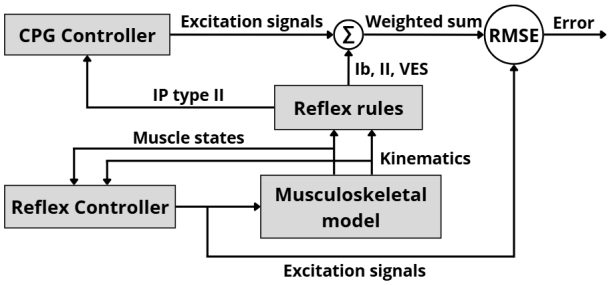

Fig. 3. Mimicking process. Block diagram of the process used to compute the RMSE between excitation signals generated by the reflex controller and the weighted sum of CPG excitation, muscle reflexes and vestibular feedback signals.

During the mimicking step, the reflex controller actively drives the musculoskeletal model, while the CPG is simulated in parallel and entrained to the musculoskeletal model via IP length feedback. Only parameters governing neuron dynamics , CPG coupling and the TA length offset were optimized, reducing the parameter space to 37 parameters for the UBG controller and 59 parameters for the TLU controller. All remaining parameters were either fixed (reference torso angle) or determined analytically using the Moore-Penrose pseudoinverse in Eqs. 12 to 14 (motor neuron, muscle reflex and vestibular feedback weights), with y_n representing the reference excitation at time n and x_{nm} denotes the m_{th} contributing signal at time n.

For example, the HAM excitation is represented as a weighted sum of H-E and K-F neuron outputs, vestibular feedback and type Ib and II muscle reflex signals. Using this method, six optimal weights are determined.

$$\begin{bmatrix} w_{opt,1} \\ \vdots \\ w_{opt,m} \end{bmatrix} = (X^T X)^{-1} X^T y \tag{12}$$

With

$$X = \begin{bmatrix} x_{1,1} & \dots & x_{1,m} \\ \vdots & \ddots & \vdots \\ x_{n,1} & \dots & x_{n,m} \end{bmatrix} \tag{13}$$

$$y = \begin{bmatrix} y_1 \\ \vdots \\ y_n \end{bmatrix} \tag{14}$$

The result from the mimic optimization was used as the initial guess for the second optimization step in which the performance measures (Section 3.7.1) were minimized. The parameter space was substantially larger in this step, as the reference torso angle and the motor

neuron, muscle reflex and vestibular feedback weights were now optimized as well.

3.7.3. Initial conditions

The initial states of the CPG neurons and the musculoskeletal system must also be specified. Ideally, these states are initialized on or close to the eventual periodic solution. Since this solution is not known a priori, the musculoskeletal model is initially controlled by the reflex controller to generate a steady gait. During this phase, the CPG is simulated in parallel and allowed to converge to a limit cycle, synchronized to the musculoskeletal model via IP type II feedback. Once stable periodic behavior is achieved, control is switched from the reflex controller to the CPG.

3.7.4. Final solution

The optimal result obtained from the two-step optimization procedure was not necessarily used for further analysis. First, the robustness of the solution was assessed by varying the time at which control was switched from the reflex controller to the CPG, essentially changing the initial conditions. A solution was considered sufficiently robust if the biped reached a stable gait cycle for multiple switching times. If the biped failed to maintain stability for multiple switch times, a solution from an earlier generation of the optimization process was selected instead. Earlier generations typically exhibit higher muscle activations, resulting in increased stiffness and reduced sensitivity to variations in initial conditions creating a robust gait cycle. This was eventually only done for the TLU model.

3.8. Gait velocity control

To assess whether the separation of frequency and amplitude in the TLU model facilitates better control of walking velocity compared to the UBG model, where these properties are coupled, three additional optimization steps were performed. The goal of each step was to maximize walking velocity by re-optimizing a subset of CPG parameter, while all other parameters were fixed at the final values obtained from the two-step optimization process described in Section 3.7. The parameters being re-optimized were:

- Step 1: tonic inputs (s_0).
- Step 2: tonic inputs (s_0) and neuron dynamics (τ_{r_i}, τ_{a_i}, and b).
- Step 3: tonic inputs (s_0), neuron dynamics τ_{r_i}, τ_{a_i}, and b, and CPG coupling weights (w_{ij}).

These parameters were selected because they determine the behavior of the CPG and, consequently, influence the frequency and amplitude of the output signals.

The objective function included the limit torque and joint angle measures, to prevent unrealistic joint kinematics, as well as the periodicity constraint (Section 3.7.1). Additionally, the same gait term was included, but with the minimum velocity set to 2 m/s. This value was chosen such that it was not reached in any of the three optimization steps. Consequently, the optimization drove the velocity towards the maximum achievable value given the set of optimizable parameters.

3.9. Validation

Validation of the two-step optimization and velocity control process was performed by comparing the simulated output to experimental normative datasets. Specifically, joint kinematics, kinetics, ground reaction forces and muscle excitations were compared with reference data taken from [26], while general spatiotemporal parameters, such as step frequency, step length and gait velocity were verified using the values reported in [27].

4. Results

This section presents the results of the two-step optimization process and the velocity control steps. Results for the UBG and TLU model from the two-step optimization include spatiotemporal gait parameters (Table III), kinematics, kinetics, ground reaction forces (Fig. 4) and muscle excitations, including the contributions of CPG signals, reflexes and vestibular feedback (Fig. 5). For the velocity control steps, only the spatiotemporal gait parameters are reported for each step Table III, while kinematics, kinetics, ground reaction forces and excitation signals can be found in Appendix B.1 to Appendix C.2. Also, videos of the solutions of the two-step optimization and the gait velocity control steps can be found in the supplementary material.

4.1. Two-step optimization

Both solutions exhibit similar gait velocities falling within the normal range, albeit toward the lower end (Table III). The UBG solution shows a slightly lower step frequency and a higher step length compared to the TLU model with the step length of the TLU being lower than normal values.

The kinematic results show good agreement with normal human gait (A1-4 in Fig. 4), with only minor deviations observed. The TLU model exhibits slightly reduced hip flexion during early stance and increased hip flexion during early swing, followed by a more pronounced extension movement at the end of the swing phase. For the knee angle, both models show little to no flexion during early stance, while the TLU model demonstrates an earlier onset of knee flexion during the swing phase. In addition, both models exhibit reduced ankle plantarflexion toward the end of stance.

Regarding the joint moments (B1-3 in Fig. 4), the hip and ankle moments generally show good agreement with normative data, although the ankle moment exhibits

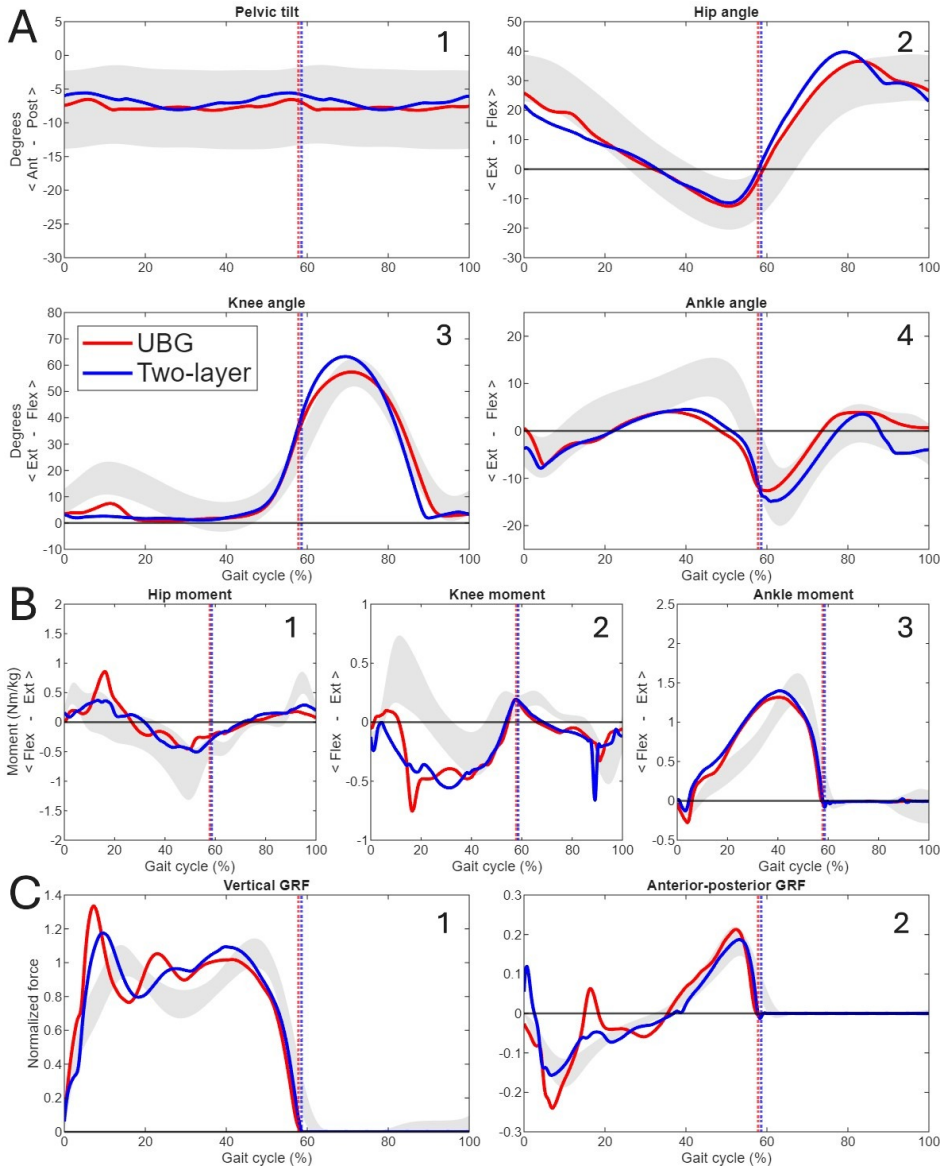

Fig. 4. Kinematics, kinetics and ground reaction forces of the two-step optimization procedure. Panels A1-4 show kinematic results, B1-3 joint kinetics and C1 and 2 ground reaction forces obtained from the two-step optimization procedure. The red line represents the UBG model and the blue line represents the TLU model. Gray bands indicate normative data within one standard deviation of the mean, based on data from [26]. Colored dotted lines indicate toe-off events. All results were time-normalized per stride; joint moments were normalized to body mass, and ground reaction forces were normalized to body weight.

a more distributed peak. In contrast, during the first part of the stance phase, the knee moment is opposite of normal data, generating a flexion moment instead. Finally, the TLU model exhibits a peak in knee flexion moment at the end of the swing phase, which can be attributed to passive structures around the knee resisting hyperextension as the shank swings forward.

The vertical and anterior–posterior components of the ground reaction force are shown in Fig. 4 C1 and 2. The anterior–posterior ground reaction force shows good agreement with normative data, particularly during the second half of the stance phase. The TLU model exhibits a large initial anterior peak, caused by excessive backward leg swing at the end of the swing phase. Finally, the UBG model shows a peak in the anterior direction during midstance.

The total muscle excitation signals and the relative contributions of the CPG, reflexes and vestibular feedback are shown in Fig. 5. When comparing the simulated excitations to normative data, the interpretation should primarily focus on activation timing (i.e., an on-off pattern), as the normalization of the normative EMG data

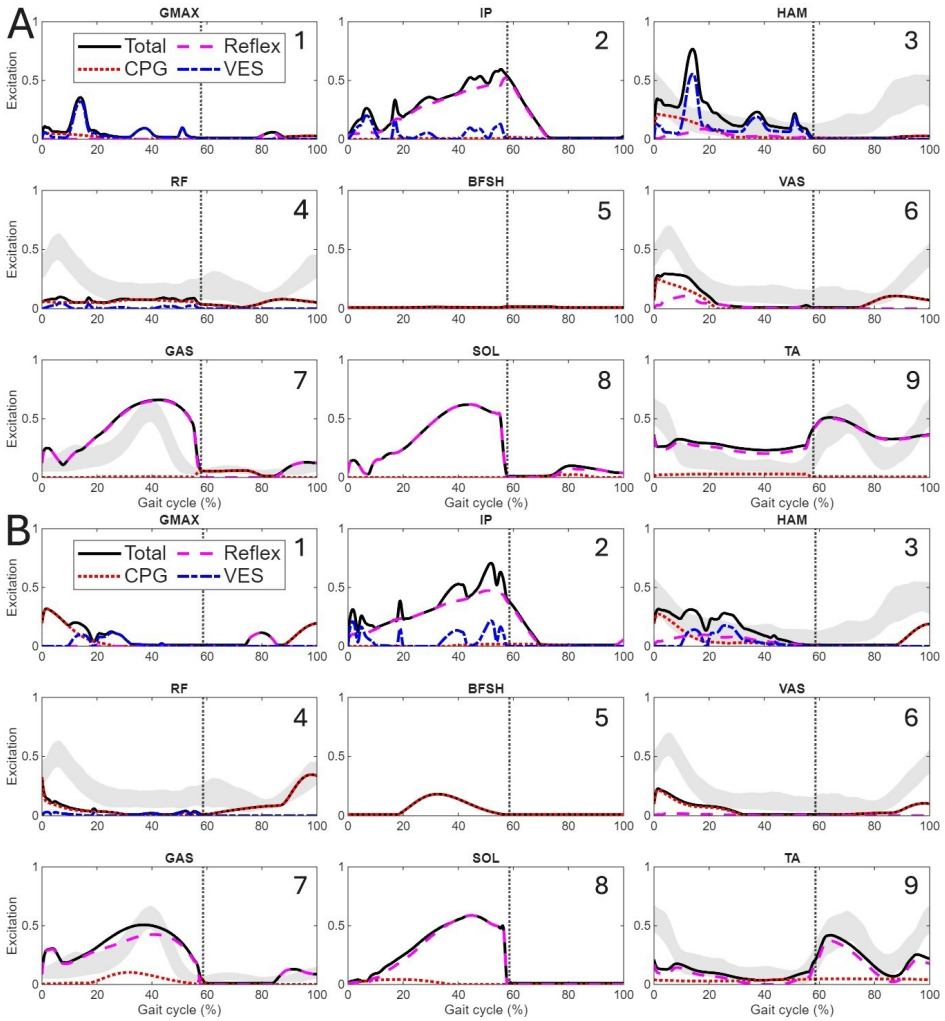

Fig. 5. Muscle excitation signals of the two-step optimization procedure. Panels A1-9 correspond to the UBG model and B1-9 to the TLU model. Black lines indicate the resulting muscle excitations, magenta dashed lines represent muscle reflex contributions, red dotted lines represent CPG signals and blue dash-dotted lines represent vestibular input. Normative data was unavailable for the GMAX, IP, BFSH, and SOL muscles. For the HAM plot, normative data from the biceps femoris muscle was used.

strongly influences the resulting amplitudes.

The total muscle excitations for the VAS, GAS, and TA in both models show similar onset timings, with a more distributed peak observed for the GAS. Additionally, the HAM and RF exhibit good agreement with normative data in the TLU model, whereas in the UBG model this agreement is only observed during the stance phase for the HAM and is poor for the RF.

In both models, the IP, GAS, SOL and TA are predominantly controlled by muscle reflexes. CPG contributions are mainly observed at the end of the swing phase and during the loading response in stance for the HAM and VAS in both models, as well as for the GMAX and RF in the TLU model. Furthermore, the BFSH shows no excitation in the UBG model, whereas slight activation during the stance phase is observed in the TLU controller. Vestibular contributions appear in an on-off like manner in the GMAX, IP, and HAM, with higher and more frequent peaks in the GMAX and HAM of the UBG model.

4.2. Velocity control

The spatiotemporal gait parameters resulting from the velocity control steps are presented in Table III. Both models were able to increase walking velocity compared to the solution from the two-step optimization process. In the UBG model, gait velocity increased by 0.13 m/s in the first control step and by 0.04 m/s in each of the two subsequent steps. Step frequency varied only minimally, with the increase in velocity coming from an increase in step length.

TABLE III

	UBG			TLU		
	Gait velocity (m/s)	Step freq. (Hz)	Step length (m)	Gait velocity (m/s)	Step freq. (Hz)	Step length (m)
Normal ranges	0.92–1.82	1.50–2.19	0.56–0.92	0.92–1.82	1.50–2.19	0.56–0.92
Two-step optimization	1.04	1.67	0.62	0.97	1.78	0.54
Velocity control step 1	1.17	1.68	0.70	1.35	1.77	0.76
Velocity control step 2	1.21	1.69	0.72	1.57	1.86	0.84
Velocity control step 3	1.25	1.67	0.75	1.67	1.96	0.86

Spatiotemporal gait parameters obtained from the two-step optimization procedure and from the three velocity control steps. Normal ranges were taken from [27]

In contrast, the TLU model exhibited a substantially larger increase in gait velocity of 0.38 m/s during the first velocity control step, exceeding the maximum velocity reached by the UBG model. This initial increase was due to an increase in step length. In the subsequent control steps, gait velocity increased further as a result of increases in both step frequency and step length.

It should be noted that the overall kinematics (Appendix B.1 and Appendix B.2 exhibit trajectories similar to those of the optimal solution, with the largest deviations observed in the knee angle and pelvic tilt. In the TLU model, the pelvis is tilted more anteriorly. Additionally, both models show an increase in the initial vertical ground reaction force peak, exceeding twice body weight.

5. Discussion

This study implemented two CPG models: the novel TLU and the conventional UBG, controlling 18 Hill-type muscles actuating a seven-segment biped during steady-state gait using only muscle reflexes and vestibular feedback signals. Both models produced similar and realistic human gait patterns, with gait velocity and step frequency falling within normal ranges. Moreover, the TLU model enabled control of gait velocity over a wider range while requiring fewer parameters compared to the UBG model.

Slight deviations from normal gait were observed in the solution from the two-step optimization process for both CPG models, which can be attributed to model simplifications. There was little to no knee flexion during the early stance phase and reduced ankle plantar flexion toward the end of the stance phase. These observations are commonly reported in predictive musculoskeletal simulations [28], [29]. The reduced knee flexion during early stance can be attributed to the effort-based cost function. Knee flexion during the loading response requires activation of the quadriceps to prevent knee collapse and may therefore be inconsistent with a minimal-effort objective. Because the knee is fully extended during this phase, a flexion moment is generated by passive structures to counteract hyperextension, whilst normally an extension moment is generated. Similarly, the reduced ankle plantarflexion during late stance may be attributed to modeling simplifications, such as modeling the foot as a single rigid segment with contact spheres and modeling ground contact using a Hunt–Crossley contact model [28], [30]. Both models exhibit a steep initial peak in the vertical component, which also is a commonly reported consequence of simplified foot and ground contact models [31].

Also, both models produced gait velocities within typical human walking ranges, although they were at the lower end. This low velocity may be caused by the two-step optimization strategy. The initial guess was derived by mimicking a reference solution generated by the Geyer and Herr reflex controller [19] and the final optimized solutions retained several of its characteristics. The Geyer and Herr model produced a gait velocity of 1.07 m/s, a step frequency of 1.79 Hz and a step length of 0.60 m, values comparable to those obtained with the UBG and TLU controllers. Therefore, the suboptimal velocity may be attributable to the optimization procedure rather than inherent limitations of the CPG models. Future work should consider initializing the optimization with a reference solution with spatio-temporal values closer to typical human gait.

To better understand the roles of the CPG, reflexes and vestibular system in motor control, muscle excitation signals were analyzed together with the relative contributions of these systems. Muscle reflexes appear to dominate motor output, particularly in the SOL, GAS, TA and IP, all four exhibiting the highest excitation levels. Reflex contributions were also present in the

HAM, VAS, and GMAX, albeit to a lesser extent. Vestibular feedback exhibited pronounced and irregular peaks. In humans, vestibular feedback influences a broad set of muscles, including those of the upper leg, lower leg and trunk [32]. In the current model, however, only four hip muscles receive vestibular input, effectively concentrating the stabilizing demands on a limited set of muscles. Additionally, the combined pelvis–torso segment is relatively large and heavy, making it more difficult to stabilize. Other models address this by separating the pelvis and torso into multiple segments [17], [33], [34] or by incorporating additional torso muscles and postural control strategies [8], [35]. Consequently, relying on a small number of muscles to stabilize a larger pelvis–torso segment likely leads to exaggerated vestibular contributions, which explains the observed abrupt peaks.

The CPG contributed substantially during the loading response by exciting the HAM, RF, VAS and GMAX at the end of swing and the onset of stance. Since the loading response is critical for preventing knee collapse and maintaining stable gait [36], this suggests an important functional role of the CPG within the present simulations. However, caution should be taken when generalizing these results to human locomotion motor control. In the current model, no reflex pathways were included which could excite the muscles during and in preparation for the load response, which resulted in the CPG taking over. Similarly, the strong reflex contributions in GAS, SOL, and TA may reflect the relatively large number of reflex pathways in these muscles. These findings therefore depend strongly on modeling choices. While no definitive conclusions can be drawn regarding the precise muscle-specific role of the CPG in humans, the results demonstrate that the CPG can generate excitation patterns in concert with reflexes and vestibular feedback, all systems complementing each other and creating a functionally redundant control architecture.

The velocity control experiments further support this interpretation. In the TLU model, substantial increases in gait velocity were achieved by optimizing only the tonic inputs to the neurons, while reflex and vestibular parameters remained fixed. Notably, the maximum velocity achieved by the UBG model after re-optimizing 36 parameters in velocity control step 3 remained lower than the velocity obtained by optimizing only ten tonic input parameters in velocity control step 1 in the TLU model.

Moreover, increases in velocity in the TLU model resulted from changes in both step frequency and step length, whereas the UBG model primarily modulated step length. In human walking, increases in velocity arise from coordinated increases in both step frequency and step length. It has been shown that the walk ratio (step length divided by step frequency) remains relatively constant across a wide range of speeds [37]. Therefore, the combined modulation of step frequency and step length observed in the TLU model is more consistent with human gait. These findings further suggest that decoupling frequency and amplitude control enables more versatile gait modulation with fewer parameters. Nevertheless, deviations in kinematics, kinetics and ground reaction forces compared to normal human gait occurred more at higher velocities, indicating that other control structures help in shaping the final gait pattern. Further work is needed to identify which model components or parameter configurations yield more realistic high velocity gaits.

6. Limitations and future work

Several additional limitations, not yet discussed, should be considered when interpreting the results.

The original TLU model of Rybak et al. [13] incorporates multiple feedback pathways to the CPG, establishing a strong coupling between the CPG and musculoskeletal system. In the present study, only type II feedback from the IP muscle during stance was included. The limited coupling may partly explain the sensitivity of the optimized solutions to small changes in initial conditions, causing the model not reach a stable gait cycle. Future implementations of this model should investigate stronger and more feedback integration with the CPG.

The musculoskeletal model was two-dimensional, relatively simple and based on a single man, including only a limited set of type II and Ib reflexes. Extending the model to three dimensions would increase complexity substantially; therefore, further refinement of the two-dimensional model is recommended. Improvements could include separating pelvis and torso segments, adding trunk musculature for enhanced postural control, implementing a more realistic foot-ground contact model and incorporating type Ia reflex pathways.

The optimization strategy relied on predefined steps, but lacked systematic tuning of parameter ranges, standard deviations and iteration counts. Many settings were determined by trial and error. While adequate solutions were obtained, a more structured optimization framework could better explore the parameter space, approach global minima and reduce computation time, which exceeded three hours for some optimizations.

7. Conclusion

This study implemented and evaluated a two-layered CPG architecture (TLU) that separates frequency and amplitude of neural output signals in a simple, two-dimensional musculoskeletal model using exclusively muscle reflexes and vestibular feedback. Both the TLU and the UBG controllers produced physiologically plausible gait patterns, with deviations largely attributable to modelling simplifications.

The results demonstrate that CPG activity can operate in conjunction with reflex and vestibular systems, complementing each other and creating a functionally redundant control system. Furthermore, the two-layer architecture of the TLU model enables more flexible modulation of gait velocity compared to the UBG model, particularly through independent control of frequency and amplitude.

References

[1] T. G. Brown, "The intrinsic factors in the act of progression in the mammal," vol. 84, no. 572, pp. 308–319, 1911.

[2] P. A. Guertin, "The mammalian central pattern generator for locomotion," *Brain Research Reviews*, vol. 62, no. 1, pp. 45–56, 2009.

[3] M. MacKay-Lyons, "Central pattern generation of locomotion: A review of the evidence," *Physical Therapy*, vol. 82, no. 1, pp. 69–83, 2002.

[4] E. Marder and D. Bucher, "Central pattern generators and the control of rhythmic movements," *Current Biology*, vol. 11, no. 23, pp. R986–R996, 2001.

[5] M. R. Dimitrijevic, Y. Gerasimenko, and M. M. Pinter, "Evidence for a spinal central pattern generator in humans," *Annals of the New York Academy of Sciences*, vol. 860, no. 1, pp. 360–376, 1998.

[6] K. Minassian, U. S. Hofstoetter, F. Dzeladini, P. A. Guertin, and A. Ijspeert, "The human central pattern generator for locomotion: Does it exist and contribute to walking?" *The Neuroscientist*, vol. 23, no. 6, pp. 649–663, 2017.

[7] G. Taga, "A model of the neuro-musculo-skeletal system for human locomotion: I. emergence of basic gait," *Biological Cybernetics*, vol. 73, no. 2, pp. 97–111, 1995.

[8] K. Hase and N. Yamazaki, "Computer simulation study of human locomotion with a three-dimensional entire-body neuro-musculo-skeletal model (i. acquisition of normal walking)," *JSME International Journal, Series C: Mechanical Systems, Machine Elements and Manufacturing*, vol. 45, no. 4, pp. 1040–1050, 2002.

[9] Y. Itoh, K. Taki, S. Kato, and H. Itoh, "A stochastic optimization method of CPG-based motion control for humanoid locomotion," 2004, pp. 347–351.

[10] C. Paul, M. Bellotti, S. Jezernik, and A. Curt, "Development of a human neuro-musculo-skeletal model for investigation of spinal cord injury," *Biological Cybernetics*, vol. 93, no. 3, pp. 153–170, 2005.

[11] W. Duan, W. Chen, J. Wang, J. Zhang, W. Chen, and Z. Zhao, "Bio-inspired control of lower limb exoskeleton using a central pattern generator," 2020, pp. 2041–2046.

[12] D. Ichimura, H. Hobara, G. Hisano, T. Maruyama, and M. Tada, "Acquisition of bipedal locomotion in a neuromusculoskeletal model with unilateral transtibial amputation," *Frontiers in Bioengineering and Biotechnology*, vol. 11, 2023.

[13] D. A. McCrea and I. A. Rybak, "Organization of mammalian locomotor rhythm and pattern generation," *Brain Research Reviews*, vol. 57, no. 1, pp. 134–146, 2009.

[14] K. E. Zelik, V. La Scaleia, Y. P. Ivanenko, and F. Lacquaniti, "Can modular strategies simplify neural control of multidirectional human locomotion?" *Journal of Neurophysiology*, vol. 111, no. 8, pp. 1686–1702, 2014.

[15] Y. P. Ivanenko, R. E. Poppele, and F. Lacquaniti, "Motor control programs and walking," *The Neuroscientist*, vol. 12, no. 4, pp. 339–348, 2006.

[16] E. Bizzi, V. Cheung, A. d'Avella, P. Saltiel, and M. Tresch, "Combining modules for movement," *Brain Research Reviews*, vol. 57, no. 1, pp. 125–133, 2008.

[17] J. Nassour, P. Hénaff, F. Benouezdou, and G. Cheng, "Multi-layered multi-pattern CPG for adaptive locomotion of humanoid robots," *Biological Cybernetics*, vol. 108, no. 3, pp. 291–303, 2014.

[18] M. Abedi, M. Moghaddam, and S. Firoozabadi, "A full bio-inspired bipedal gait locomotion system," 2014, pp. 178–184.

[19] H. Geyer and H. Herr, "A muscle-reflex model that encodes principles of legged mechanics produces human walking dynamics and muscle activities," *IEEE Transactions on Neural Systems and Rehabilitation Engineering*, vol. 18, no. 3, pp. 263–273, 2010.

[20] T. Geijtenbeek, "SCONE: Open source software for predictive simulation of biological motion," vol. 4, no. 38, p. 1421, 2019. [Online]. Available: http://joss.theoj.org/papers/10.21105/joss.01421

[21] G. Taga, Y. Yamaguchi, and H. Shimizu, "Self-organized control of bipedal locomotion by neural oscillators in unpredictable environment," vol. 65, no. 3, pp. 147–159, 1991.

[22] K. Matsuoka, "Mechanisms of frequency and pattern control in the neural rhythm generators," vol. 56, no. 5, pp. 345–353, 1987.

[23] ——, "Sustained oscillations generated by mutually inhibiting neurons with adaptation," vol. 52, no. 6, pp. 367–376, 1985.

[24] E. Van Der Kruk and T. Geijtenbeek, "A planar neuromuscular controller to simulate compensation strategies in the sit-to-walk movement," vol. 19, no. 6, 2024.

[25] J. M. Wang, S. R. Hamner, S. L. Delp, and V. Koltun, "Optimizing locomotion controllers using biologically-based actuators and objectives," vol. 31, no. 4, pp. 1–11, 2012.

[26] T. Van Criekinge, W. Saeys, S. Truijen, L. Vereeck, L. H. Sloot, and A. Hallemans, "A full-body motion capture gait dataset of 138 able-bodied adults across the life span and 50 stroke survivors," vol. 10, no. 1, p. 852, 2023.

[27] F. R. Finley and K. A. Cody, "Locomotive characteristics of urban pedestrians," vol. 51, no. 7, pp. 423–426, 1970.

[28] A. Falisse, M. Afschrift, and F. De Groote, "Modeling toes contributes to realistic stance knee mechanics in three-dimensional predictive simulations of walking," vol. 17, no. 1, 2022.

[29] M. Ackermann and A. J. Van Den Bogert, "Optimality principles for model-based prediction of human gait," vol. 43, no. 6, pp. 1055–1060, 2010.

[30] L. D'Hondt, F. De Groote, and M. Afschrift, "A dynamic foot model for predictive simulations of human gait reveals causal relations between foot structure and whole-body mechanics," vol. 20, no. 6, p. e1012219, 2024.

[31] M. Denayer, E. Alfio, M. A. Díaz, M. Sartori, F. De Groote, K. De Pauw, and T. Verstraten, "A PRISMA systematic review through time on predictive musculoskeletal simulations," vol. 22, no. 1, p. 149, 2025.

[32] A. S. Ali, K. A. Rowen, and J. F. Iles, "Vestibular actions on back and lower limb muscles during postural tasks in man," vol. 546, no. 2, pp. 615–624, 2003.

[33] W. Yu and Y. Ikemoto, "An artificial reflex improves the perturbation-resistance of a human walking simulator," vol. 45, no. 11, pp. 1095–1104, 2007.

[34] N. Van Der Noot, A. J. Ijspeert, and R. Ronsse, "Bio-inspired controller achieving forward speed modulation with a 3d bipedal walker," vol. 37, no. 1, pp. 168–196, 2018.

[35] Y. Kim, Y. Tagawa, G. Obinata, and K. Hase, "Robust control of CPG-based 3d neuromusculoskeletal walking model," vol. 105, no. 3, pp. 269–282, 2011.

[36] P. R. G. Lucareli and J. M. D. Greve, "Alteration of the load-response mechanism of the knee joint during hemiparetic gait

following stroke analyzed by 3-dimensional kinematic," vol. 61, no. 4, pp. 295–300, 2006.
[37] N. Sekiya and H. Nagasaki, "Reproducibility of the walking patterns of normal young adults: test-retest reliability of the walk ratio(step-length/step-rate)," vol. 7, no. 3, pp. 225–227, 1998.

Appendix A

Definition of the cost of transport (CoT)

$$\dot{E} = \dot{A} + \dot{M} + \dot{S} + \dot{W} \tag{15}$$

With $\dot{E}$ as the metabolic energy expenditure, $\dot{A}$ as the muscle activation heat rate, $\dot{M}$ is the muscle maintenance heat rate, $\dot{S}$ is the muscle shortening heat rate and $\dot{W}$ is the positive mechanical work rate.

$$\dot{A} = \text{mass} \cdot f_A(u) \tag{16}$$

With

$$f_A(u) = 40\lambda \sin\left(\tfrac{\pi}{2}u\right) + 133(1-\lambda)\left(1 - \cos\left(\tfrac{\pi}{2}u\right)\right) \tag{17}$$

λ denotes the fraction of Type I fibers in a given muscle and mass is the muscle mass.

$$\dot{M} = \text{mass} \cdot g(\hat{l}^{CE}) f_M(a) \tag{18}$$

With

$$f_M(a) = 74\lambda \sin\left(\tfrac{\pi}{2}a\right) + 111(1-\lambda)\left(1 - \cos\left(\tfrac{\pi}{2}a\right)\right) \tag{19}$$

$$g(\hat{l}^{CE}) = \begin{cases} 0.5, & \text{if } 0.0 < \hat{l}^{CE} \leq 0.5 \\ \hat{l}^{CE}, & \text{if } 0.5 < \hat{l}^{CE} \leq 1.0 \\ -2\hat{l}^{CE} + 3, & \text{if } 1.0 < \hat{l}^{CE} \leq 1.5 \\ 0, & \text{if } 1.5 < \hat{l}^{CE} \end{cases} \tag{20}$$

$\hat{l}^{CE}$ is the normalized muscle fiber length.

$$\dot{S} = 0.25 \cdot F^{MTU} \left\{-v^{CE}\right\}_+ \tag{21}$$

$\dot{F}^{MTU}$ is the active plus passive force of the musculotendon unit, v^{CE} is the shortening velocity of the contractile element.

$$\dot{W} = F^{CE} \left\{-v^{CE}\right\}_+ \tag{22}$$

F^{CE} is the active force produced by the contractile element.

The Cost of Transport is then defined as:

$$CoT = \frac{1}{m}\left(\dot{B} + \frac{1}{T}\sum_{t=1}^{T}\sum_{m\in\mathcal{M}} \dot{E}_{m,t}\right) \tag{23}$$

$\dot{E}_{m,t}$ is the metabolic engergy expenditure for MTU m at timestep t, T is the total time, $\mathcal{M}$ is the set of all eighteen muscles, $\dot{B}$ is the metabolic energy rate, set to 1.51 times body mass and m is the total distance walked.

Appendix B.1

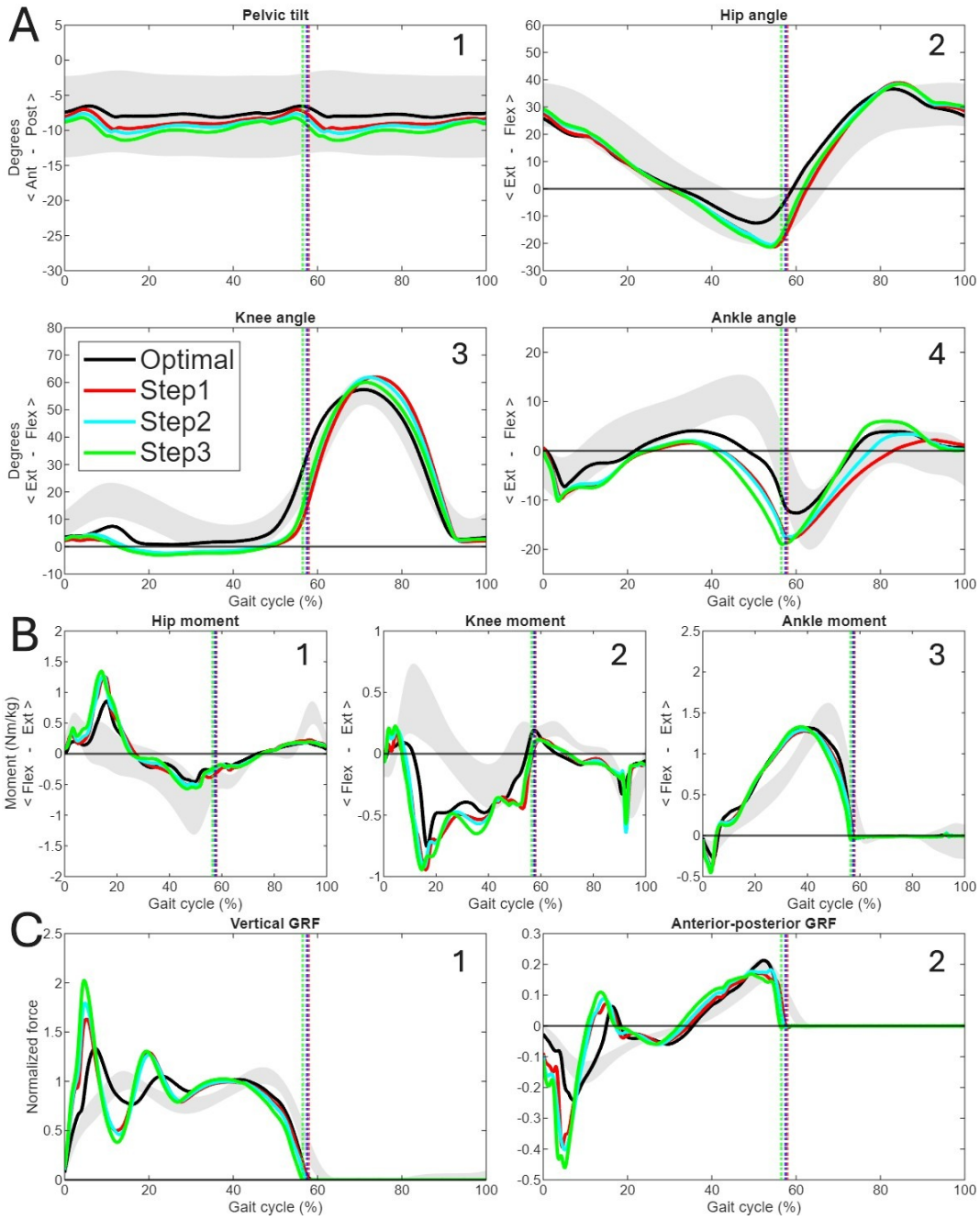

Fig. 6. Kinematics, kinetics and ground reaction forces from the two-step optimization process and the velocity control steps for the UBG model. A1-4 show kinematic results, B1-3 joint kinetics and C1 and 2 show ground reaction forces obtained from the three steps during the velocity control procedure. The red line represents step 1, blue step 2 and green step 3. Gray bands indicate normative data within one standard deviation of the mean. Colored dotted lines indicate toe-off events. All results were time-normalized per stride; joint moments were normalized to body mass, and ground reaction forces were normalized to body weight.

Appendix B.2

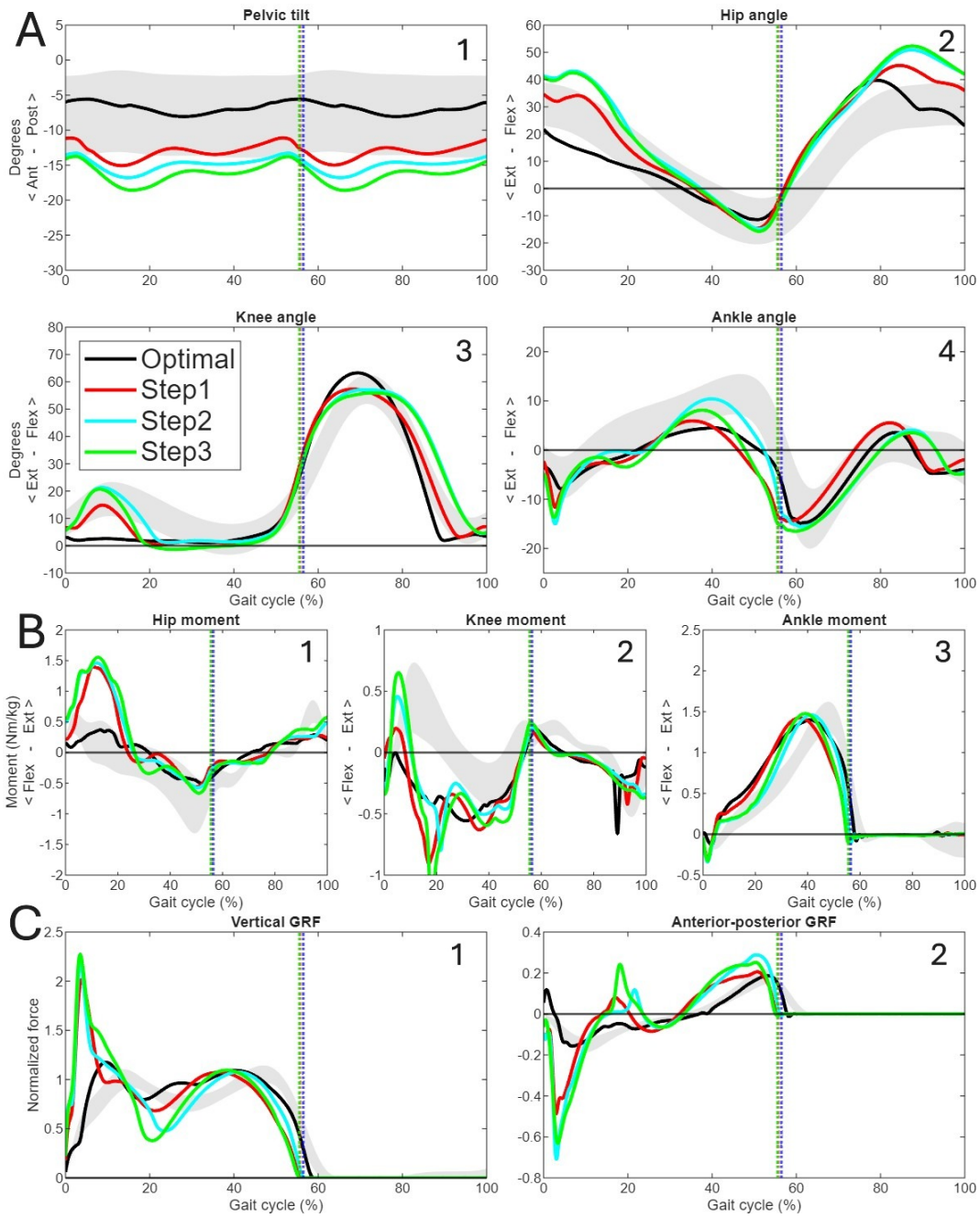

Fig. 7. Kinematics, kinetics and ground reaction forces from the two-step optimization process and the velocity control steps for the TLU model. A1-4 show kinematic results, B1-3 joint kinetics and C1 and 2 show ground reaction forces obtained from the three steps during the velocity control procedure. The red line represents step 1, blue step 2 and green step 3. Gray bands indicate normative data within one standard deviation of the mean. Colored dotted lines indicate toe-off events. All results were time-normalized per stride; joint moments were normalized to body mass, and ground reaction forces were normalized to body weight.

Appendix C.1

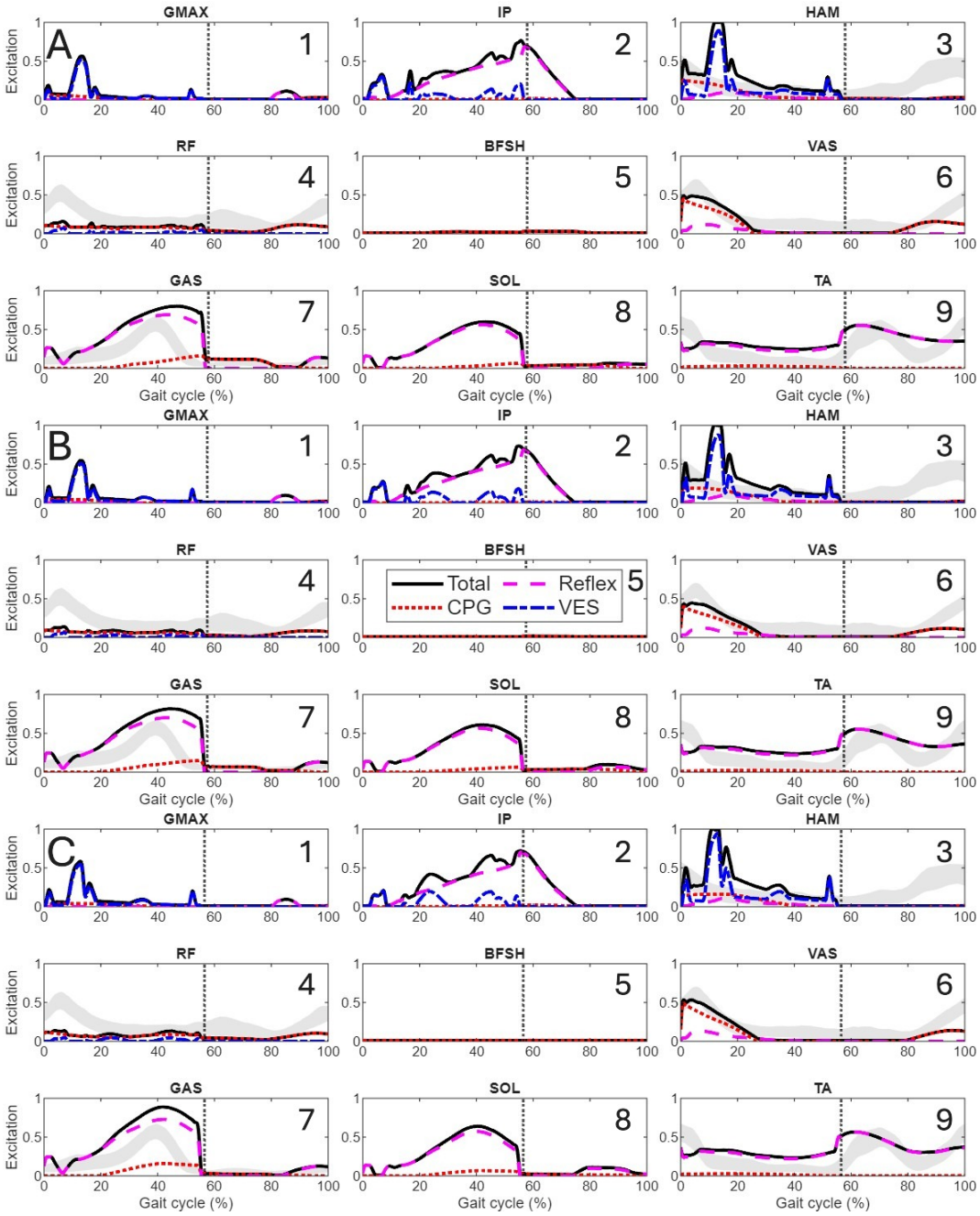

Fig. 8. Excitation signals from the velocity control steps for the UBG model. Total muscle excitation signals and the contributions of different excitation sources obtained from the three steps during the velocity control procedure. Panels A1-9 correspond to step 1, B1-9 to step 2 and C1-9 to step 3. Black lines indicate the resulting muscle excitations, magenta dashed lines represent muscle reflex contributions, red dotted lines represent CPG signals and blue dash-dotted lines represent vestibular input. Normative data was unavailable for the GMAX, IP, BFSH, and SOL muscles. For the HAM plot, normative data from the biceps femoris muscle was used.

Appendix C.2

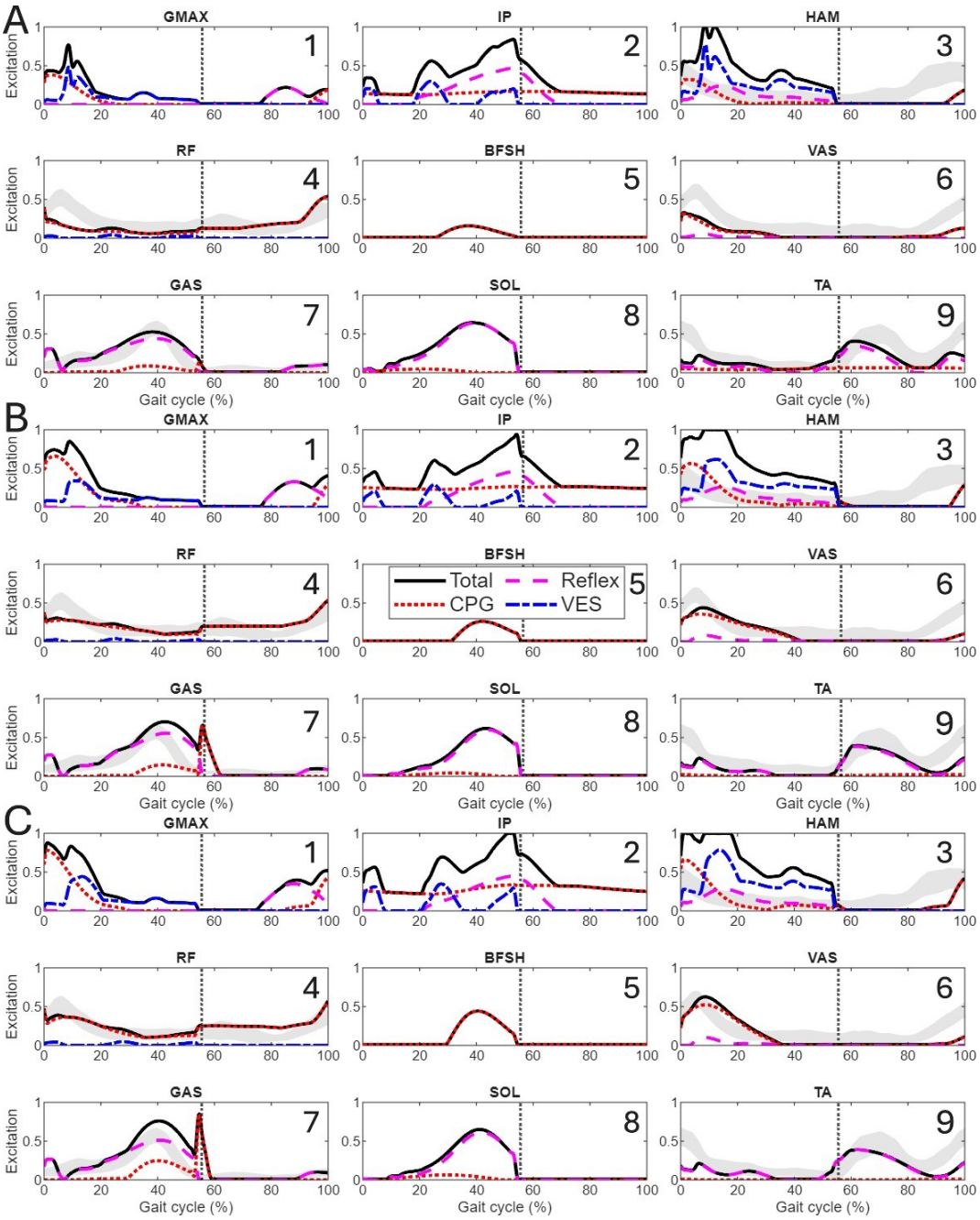

Fig. 9. Excitation signals from the velocity control steps for the TLU model. Total muscle excitation signals and the contributions of different excitation sources obtained from the three steps during the velocity control procedure. Panels A1-9 correspond to step 1, B1-9 to step 2 and C1-9 to step 3. Black lines indicate the resulting muscle excitations, magenta dashed lines represent muscle reflex contributions, red dotted lines represent CPG signals and blue dash-dotted lines represent vestibular input. Normative data was unavailable for the GMAX, IP, BFSH, and SOL muscles. For the HAM plot, normative data from the biceps femoris muscle was used.